Evolution of vectoring control of a primary jet with synthetic jets*

LUO Zhen-bing, XIA Zhi-xun, WANG De-quan, HU Jian-xin, MIAO Wan-bo, HUANG Li-ya

(Inst. of Aerospace and Material Engineering, National Univ. of Defence Technology, Changsha 410073, China)

Abstract The technique of jet vectoring using synthetic jets has a potential ability of thrust vectoring a primary jet, such as thrust vectoring controlling the inlet air jet and the nozzle jet of the air-breathing engine. To investigate the evolution of vectoring control of a primary jet with synthetic jets, a primary jet vectoring control using synthetic jet actuators with different exit configurations was numerically simulated and analyzed. The results show the evolution of jet vectoring using synthetic jets is divided into three stages. In the conduit of the primary jet, the low-pressure region, which results from the interaction between the synthetic jet and the primary jet, contributes to the vectoring force and leads to a turning of the primary jet at the conduit exit, and the primary jet turns Φ_{iv}. And then, in the near field, the primary jet fluid is entrained and absorbed by the synthetic jet during the blowing and the suction stroke, and the primary jet turns $\Phi_{\textcircled{n}}$. Finally, in the far field, the shear layer of primary jet is inspirited by the vortices of synthetic jet, and the primary jet turns $\Phi_{\textcircled{f}}$. So the final vectoring angle of the primary jet is a overall result of the primary jet controlled by synthetic jet at the three stages, $\Phi = \Phi_{iv} + \Phi_{\textcircled{n}} + \Phi_{\textcircled{f}}$.

Key words Flow control; Vectoring control*; Synthetic jet*; Vectoring angle*; Numerical simulation

中图分类号: V211.3 **文献标识码**: A **文章编号**: 1001-4055 (2008) 02-0179-08

合成射流控制主流矢量的发展过程

罗振兵, 夏智勋, 王德全, 胡建新, 缪万波, 黄利亚

(国防科技大学 航天与材料工程学院, 湖南 长沙 410073)

摘 要: 合成射流激励器射流矢量控制具有对吸气式发动机进气道出流和发动机喷管流动进行矢量控制的潜力。通过对四种不同出口构型合成射流激励器控制主流矢量偏转的数值模拟和分析, 对合成射流控制主流矢量的发展过程进行了研究。结果表明: 合成射流控制主流矢量的发展过程可分为三个不同阶段. 第一阶段. 在主流通道内, 激励器工作引起的主流通道压强梯度形成的侧向力致偏主流, 在出口处主流矢量偏转 Φ_{iv}; 第二阶段, 在主流出口附近, 合成射流对主流的卷吸作用和引射作用, 致偏主流 $\Phi_{\textcircled{n}}$; 第三阶段, 在出口下游, 合成射流与主流自由剪切层发生相互耦合作用, 致偏 $\Phi_{\textcircled{f}}$。因此, 主射流最终偏转角度 Φ是其在经历三个不同阶段时受到的合成射流致偏作用之和, 即 $\Phi = \Phi_{iv} + \Phi_{\textcircled{n}} + \Phi_{\textcircled{f}}$。

关键词: 流量控制; 矢量控制*; 合成射流*; 矢量角; 数值仿真

1 Introduction

Thrust vectoring is an innovative technology that enhances the projection of aerospace power with many advantages, including improved aircraft maneuverability, performance, survivability, and stealth. Mechanical thrust-vectoring designs, however, have proven to be heavy, complex, expensive, and counter-productive to stealth. Fluidics may offer reduced weight, higher reliability, and stealth compatibility[1]. Among the fluidics, flow control approaches that use synthetic jets have become an important tool for the aerodynamicist. Synthetic

* 收稿日期: 2006-10-28; 修订日期: 2007-06-18。
基金项目: 国家自然科学基金重大研究计划资助项目 (90205016); 国家自然科学基金项目 (50176055); 国防科技大学博士创新资助重点项目。
作者简介: 罗振兵 (1979—), 男, 博士, 研究领域为流动控制技术及固体火箭技术。E-mail: luozhenbing@163.com

jets utilize alternating suction and blowing through a slot or hole to create a boundary condition with zero net mass flux but with momentum transfer to the flow. The unique characteristics of the synthetic jets make the synthetic jet actuators suitable for a large class of applications[2~15], especially jet vectoring control. The technique of jet vectoring control using synthetic jets has a potential ability of thrust vectoring a primary jet, such as thrust vectoring controlling the inlet air jet and the nozzle jet of the air-breathing engine.

The former studies have shown the jet vectoring using synthetic jets is promising[4~11]. However, none of these studies have focused on the evolution of vectoring control of a primary jet with synthetic jets. And the understanding the evolution of vectoring control of a primary jet with synthetic jets is a base of modeling a quantitative model of vectoring control of a primary jet with synthetic jets.

In this study, the interactions between a primary air jet and four types of actuator with different exits are numerically simulated. Based on analyzing the computational results, the evolution of vectoring control of a primary jet with synthetic jets is investigated.

2 Numerical simulation

2.1 Configuration of actuator exit

Figure 1 shows the schematic of the near-exit configuration of the synthetic jet actuators with four exit modes: even exit, step exit, slope exit, and slope-step exit. The slope angle θ is defined as the angle between the centerline of the primary jet conduit and the exit slot wall of the synthetic jet. The step length s is defined as the one-sided extension of the actuator exit. The width of the exit slot and the distance from the synthetic jet to the priamry jet are fixed in all of the simulations, that is, $h = 1$ mm and $d = 4$ mm, respectively.

2.2 Computational method and validation

An incompressible flow solver, INS2D is used for the simulations at very low Mach numbers. The incompressible code has the advantage of running more efficiently than a compressible code, since compressible codes which run at very low Mach numbers require very small time steps to maintain stability. Accordingly, the unsteady, incompressible, Reynolds-averaged Navier-Stokes (RANS) equations are solved. The turbulence model used is based on the k-ε model.

X-L model[16], a computational model for synthetic jet actuator is adopted which considers the actuator cavity and the exit throat as a single computational domain. The actuator diaphragm is excited electrically by voltage; f is a forcing frequency, A denotes the amplitude of the vibrating metal diaphragm, r is the radius of the metal diaphragm, and Φ_0 is the original phase of the actuator diaphragm. For an arbitrary point on the diaphragm (y, l), here l is the distance from the point to the center of the diaphragm. The velocity of this point is composed of axial velocity $u_y(l, t)$ and radial velocity $u_l(l, t)$. Provided the diaphragm vibrates in cosine form and the function is given as follows

$$\begin{cases} u_y(l, t) = 2\pi f A \cdot \left| 1 - \dfrac{l^2}{r^2} \right| \cdot \sin(2\pi f t + \varphi_0) \\ u_l(l, t) \approx 0 \end{cases} \tag{1}$$

For the present application, $f = 500$ Hz, $A = 0.2$ μm, $r = 25$ mm, and $\varphi_0 = 0$.

The computational domain and grid of synthetic jet

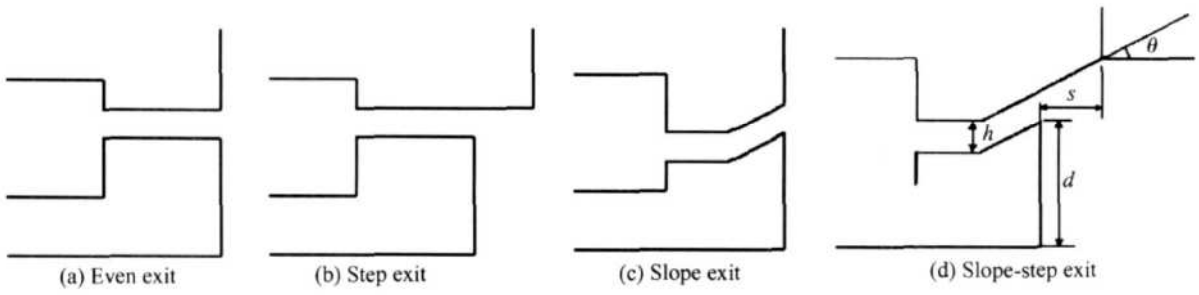

Fig 1 Schematics of the near-exit configuration of the synthetic jet actuators

actuator are illustrated in Figure 2. An inflow boundary was specified along the actuator membrane as Eq. (1). And a velocity inlet condition was adopted along the primary jet inlet boundary. Outflow conditions were employed along the free boundaries, and no-slide wall conditions were applied along the solid walls.

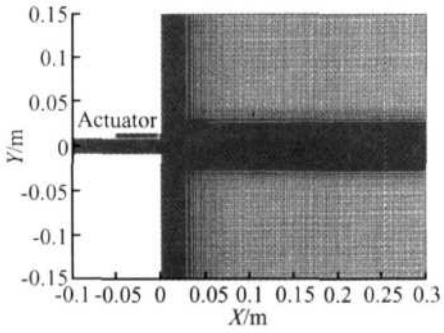

Fig. 2 Computational domain and grid

The numerical simulation of a single synthetic jet in quiescent air was validated in former work [14]. For the similar conditions of jet vectoring using synthetic jets as the experiment in the literature [4], the flow field was numerical simulated in the former study [17]. The comparison between the experiment and numerical simulation is shown in Figure 3. The vectoring angle in the numerical simulation shown in Figure 3(b) is of the same order as in the experiment shown in Figure 3(a). And the numerical accuracy is validated.

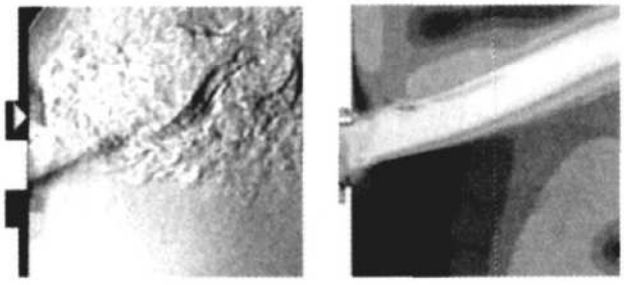

Fig. 3 Comparison between experiment and simulation

2.3 Computational results

The computational cases are summarized in Table 1. The width of the primary jet conduit H = 16 mm, for the baseline Case 0, at the primary jet conduit exit, the cross-stream averaged velocity is U_{ave} = 19.6 m/s, the conduit Reynolds number is $Re_H = U_{ave}H/\nu$ = 21 400, where ν is the kinematic viscosity. The synthetic jets in quiescent air at the condition of four types of actuator with different exits are simulated in Case1 ~ 4. Four representative cases for the interaction between the primary jet and four types actuator with different exit are discussed in Case 5~ 8. The configuration parameters of the actuator exit are expressed in Table1.

Table1 Computational cases for jet vectoring

Case	U_{ave} / (m/s)	s/h	θ/ (°)	Actuator
Case 0	19.6	0	0	Off
Case 1	0	0	0	On
Case 2	0	2	0	On
Case 3	0	0	27	On
Case 4	0	2	27	On
Case 5	19.6	0	0	On
Case 6	19.6	2	0	On
Case 7	19.6	0	27	On
Case 8	19.6	2	27	On

Figure 4 shows time locked velocity traces on the centerline of synthetic jet with different exits at X/h = 0, where the subscript $u_1(t)$ is the centerline velocity on the actuator exit. It demonstrates that the velocity $u_1(t)$ can be approximatively formulated in a sinusoidally varying profile of the form

$$u_1(t) = u_{amp}\sin(2\pi ft) = u_{amp}\sin(2\pi t^*) \quad (2)$$

where dimensionless time $t^* = t/T$-N, and $T = 1/f$, N is the actuation circles.

The stroke length of synthetic jet was introduced as follows

$$L = \int_0^{T/2} u_1(t)\,dt \quad (3)$$

And the x-coordinate component of the stroke length of synthetic jet is

$$L_0 = L\cdot\cos\theta = \int_0^{T/2} u_1(t)\cos\theta dt \quad (4)$$

Substituting Eq. (2), θ= 27°, and the data in Figure 4 into Eq. (4) results in L_0 = 25 mm for actuators with

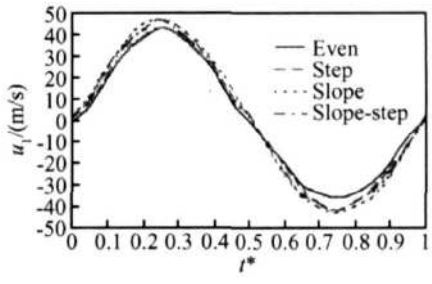

Fig. 4 Time locked velocity traces on centerline of synthetic jets per unit circle at X/h = 0

four mode exits

Figure 5 shows the path lines of the primary jet vectoring with synthetic jets for Case 5~ 8 Although the primary jet and the synthetic jet are given fixed, the vectoring angles of primary jet are different controlled by the actuator with different exits And the vectoring angle of primary jet is the largest one under the actuator with slope-step exit

Figure 6 shows the contour maps of relative pressure ($p - p_0$, p_0 is operating pressure) around the conduit at the blowing instant $t^* = 0.375$ and suction instant $t^* = 0.625$ for Case 5~ 8 There is a lower pressure region between the synthetic jet and the primary jet that results from their interaction

3 Evolution of vectoring control of a primary jet with synthetic jets

3.1 In the primary jet conduit ($X/h \leqslant 0$)

The lower pressure region contributes to the vectoring force and leads to a turning of the primary jet at the conduit exit Figure 7 shows the relative pressure along the down-wall and up-wall of the primary jet conduit at the blowing instant $t^* = 0.375$ and suction instant $t^* = 0.6255$ The pressure data in Figure 7 show that most of the contribution to vectoring force in the conduit occurs within the domain $-2 \leqslant X/h \leqslant 2$ It also shows that the relative pressure is almost unaltered at different instant times, so the primary jet-vectoring angle Φ_1 at the conduit exit ($X = 0$) is almost unaltered at different instant times

The resulting vectoring force $F_y(x)$ is computed for the domain $-2 \leqslant X/h \leqslant 2$ by the pressure difference between the upper and lower walls as follows

$$F_y(0) = \int_{-2h}^{0} [p_d(x) - p_u(t)]\,dx \qquad (5)$$

where $p_d(x)$ and $p_u(x)$ are the relative pressure along the down-wall and up-wall of the primary jet conduit respectively

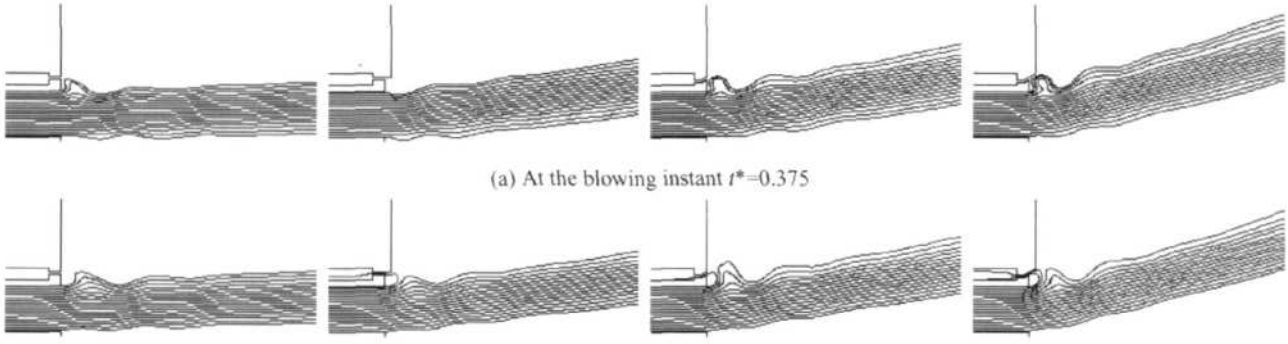

(a) At the blowing instant t^*=0.375

(b) At the suction instant t^*=0.6255

Fig. 5 Path lines of the primary jet for Case 5 ~ 8

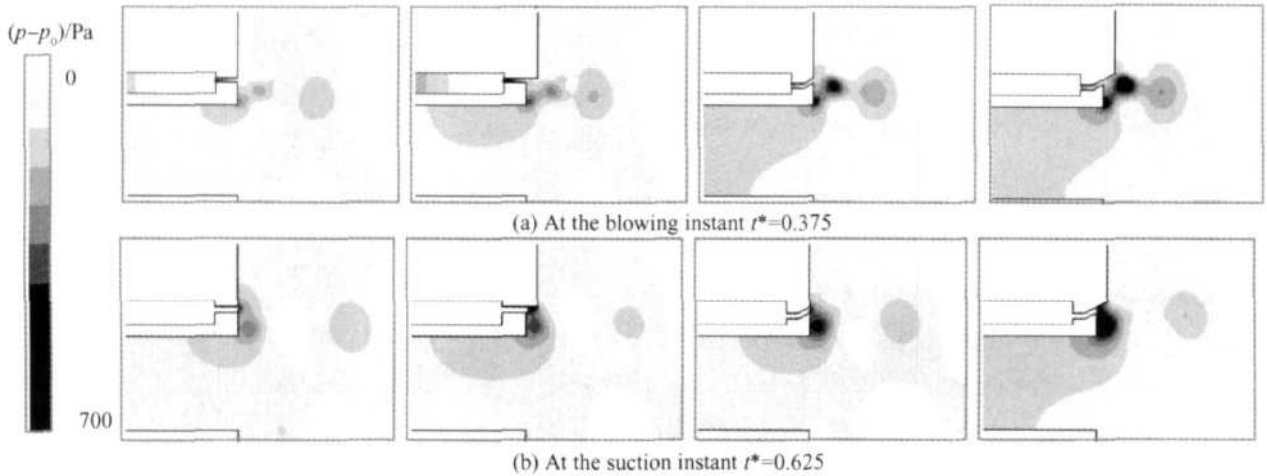

(a) At the blowing instant t^*=0.375

(b) At the suction instant t^*=0.625

Fig. 6 Contours of pressure relative maps around the jets for Case 5 ~ 8

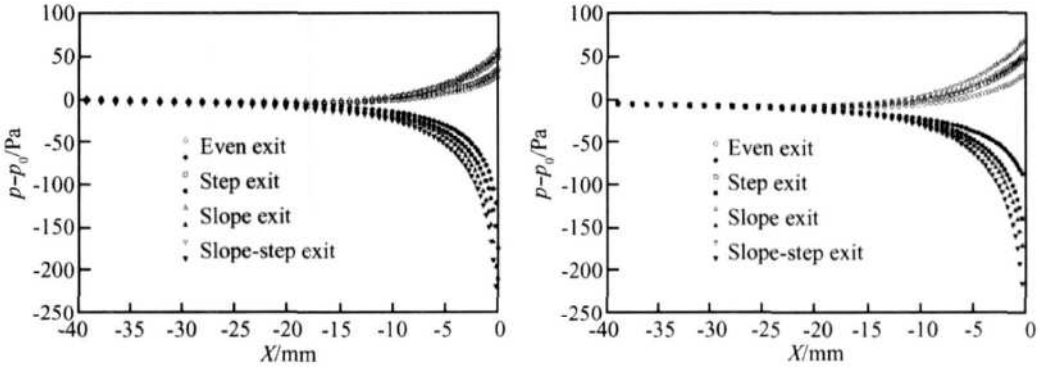

Fig 7 Pressure along the walls of primary jet conduit for Case 5~ 8 Open and closed symbols correspond to pressure along the down-and up-wall of the primary jet conduit

The net flux of streamwise momentum and cross-stream momentum of the primary jet on the conduit exit ($X = 0$) is

$$J_x = \int_{-H/2}^{H/2} \rho U(x, y) U(x, y)\, dy$$
$$J_y = \int_{-H/2}^{H/2} \rho U(x, y) V(x, y)\, dy \qquad (6)$$

Where $U(x, y)$ and $V(x, y)$ are the stream-wise velocity component and cross-stream velocity component, respectively.

Φ is the vectoring angle of the primary jet

$$\mathrm{tg}\Phi = \frac{V(x, y)}{U(x, y)} \qquad (7)$$

From the momentum theorem, $J_y = F_y$, and Eqs (6) and (7) induce the vectoring angle of the primary jet as follows

$$\Phi = \tan^{-1}(F_y / J_x),\ X \leq 0 \qquad (8)$$

Substituting Eq. (5) into Eq. (8), and results in the average vectoring angle Φ_1 of the primary jet at the conduit exit ($X = 0$) as follows

$$\Phi_1 = \tan^{-1}(F_y(0) / J_{x=0}) =$$
$$\tan^{-1}\left(\int_{-H}^{0} [p_d(x) - p_u(x)]\, dx / \rho H U_{ave}^2\right) \qquad (9)$$

Substituting the data in Figure 7 into Eq. (9), and the primary jet vectoring angle at the conduit exit for Case 5~ 8 are Φ_1= 3°, 5°, 6°, 8°. In general, the vectoring angle Φ_1 is not equal to the final vectoring angle of the primary jet

3.2 In the near field ($0 \leqslant X \leqslant L_0$)

During the blowing and the suction stroke, the primary jet fluid is entrained by the synthetic jet in the near field ($0 \leqslant X \leqslant L_0$). The entrainment ratio r_{En} is utilized to determine the entrainment performance of the synthetic jet flow to primary jet flow, which directly influences the vectoring angle. The entrainment ratio r_{En} is defined as

$$r_{En} = m_{ps} / m_s \qquad (10)$$

where m_{ps} is the mass rate of primary jet fluid diverted to the synthetic jet, and the primary jet fluid diverted to the synthetic jet is divided by a saddle point between two jet. m_s is the synthetic jet mass rate.

Figure 8 shows the contours of the stream function and the saddle points around the jets for Case 5 ~ 8. During the blowing stroke (for example, at the blowing instant $t^* = 0.375$, Figure 8(a)), a saddle point P formes between the two jets. The point P divides the primary jet flow into two parts: one part is entrained by the synthetic jet, the other part is advected downstream. In Figure 8(a), the entrainment ratios r_{En} for case 5, 6, 7, 8 are 7/7, 9/7, 9/7, and 10/7, respectively. It shows that the entrainment ratio r_{En} is regulated by the actuator exit extension step and slope angle, and the actator with slope-step exit entraines the primary jet fluid the most. During the suction stroke (for example, at suction instant $t^* = 0.625$, Figure 8(b)), a saddle point S is formed downsrteem the synthetic jet. The point S divides the flow into four quadrants. As shown in Figure 8(b), the entrainment ratio r_{En} for case5, 6, 7, 8 are 1/7, 3/7, 5/7 and 6/7, respectively, and r_{En} in the suction stroke is also regulated by the actuator exit extension step and slope angle. Therefore, for a given primary jet speed and synthetic jet strength, the entrainment ratio r_{En} can be regulated by the actuator exit con-

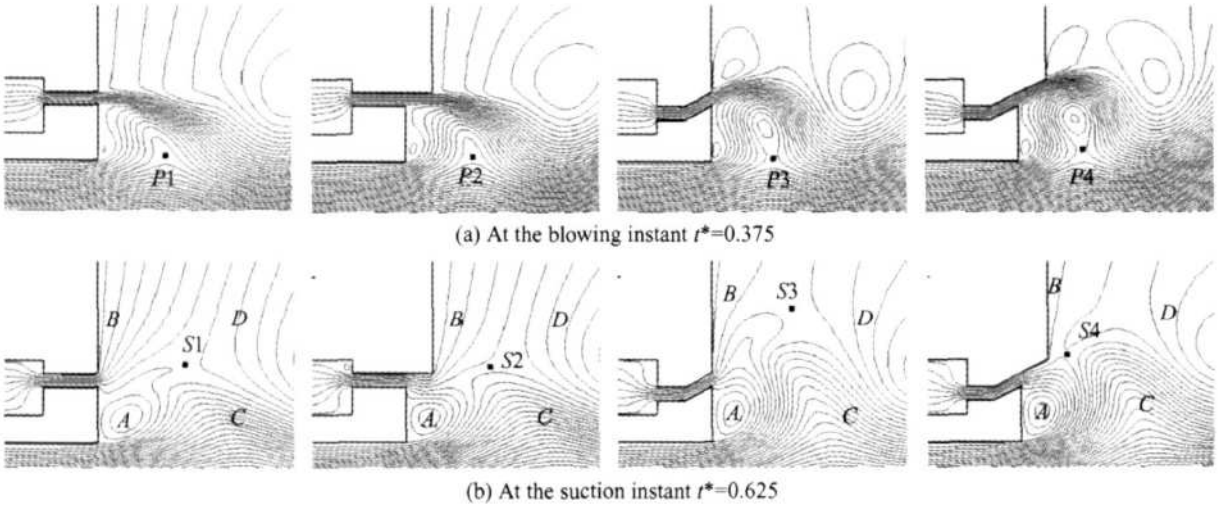

Fig 8 Contours of stream function around the jets for Case 5~ 8

figurations, and a larger jet vectoring angle Φ will be expected when the actuator adopts a slope-step exit configuration.

On the other hand, the turning of the primary jet is resisted by the actuator exit step and the synthetic jet stream-wise momentum impulse, and the slope angle increases the distance of two jets, which somewhat decreases the interaction of two jets. So, in the near field, the turning angle of the primary jet is complicated and may be a positive, zero or negative value.

3.3 In the far field ($X \geqslant L_0$)

In the far field downstream, the shear layer of primary jet is inspirited by the vortices of synthetic jet, and the primary jet turns $\Phi_{②}$. The turning angle $\Phi_{②}$ is a small value and negligible, but it may be significant when the vortices of synthetic jet near the wall, for the vortices can force the primary jet to come closer to the wall.

3.4 Evolution of jet vectoring control

Figure 9 shows velocty pofiles at downstream X = 50 mm and points of intersection with $u = 1/2U_{ave}$. And based on the data of points of intersection, the average vectoring angle of the primary downstream can be given by following equation

$$\phi_x = \tan^{-1}\left|\frac{y_- + y_+}{2x}\right|, X > 0 \qquad (11)$$

where y_- and y_+ are the coordinate values correspond to the primary jet flow velocity $u = 1/2U_{ave}$ (as shown in Figure 9).

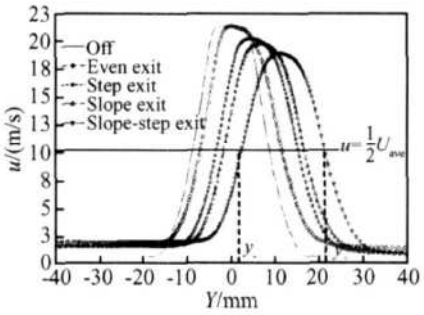

Fig 9 Velocity profiles at downsteam X = 50 mm for Case 0, 5~ 8, and points of intersection with u = 1/2 U_{ave}

For example, at X = 50 mm, the vectoring angle of the primary jet controlled by actuator with slope-step exit is $\Phi_{x=50} = \tan^{-1}[(2.4+22.4)/100] = 13.9°$. In the same way, the evolution of vectoring angle downstream can be given by substituting the data of points of intersection into Eq. (11).

Therefore, the average vectoring angle of the primary jet in the primary jet conduit ($X \leqslant 0$) and downstream ($X > 0$) can be computed from Eq. (8) and Eq. (11), respectively.

Figure 10 shows the evolution of vectoring angle Φ, which is divided into three stages. At the conduit exit X = 0, the vectoring angle of the primary jet contolled by actuators with even, step, slope exit and slope-step exit are Φ_1 = 3°, 5°, 6°, 8°. At downstream $X = L_0$ = 25 mm, the vectoring angle of the primary jet $\Phi_{x=L_0}$ = 2.6°, 6.8°, 8.6°, 13.1°. The turning angles in the near field are $\Phi_{②} = \Phi_{x=L_0} - \Phi_{iv} = -0.4°$, 1.8°,

2.6°, 5.1°. And note that the turning angle of the primary jet contolled by actuator with even exit is - 0.4°, a negative value, and the evolution curve of its vectoring angle ascends and then descends, the reason is the entrainment and absorption of primary jet fluid by the synthetic jet increasing the jet vectoring angle, but the resistance of the synthetic jet stream-wise momentum impulse downstream to the turning of the primary jet decreasing the jet vectoring angle much more. In the far field, for example, $X = 75\ \text{mm} = 3L_0$, the final vectoring angle of the primary jet for Case 5 ~ 8 are, $\phi =$ 2.5°, 7°, 9°, 14°. The turning angles in the far field ($X \geqslant L_0$) are $\phi_{\text{㈢}} = \phi - \phi_{x=L_0} =$ - 0.1°, 0.2°, 0.4°, 0.9°. Comparing $\phi_{x=L_0}$ and ϕ, and they are nearly the same, which implies the jet vectoring is nearly finished in the near field.

Therefore, the final vectoring angle of the primary jet is a total result of the primary jet controlled by synthetic jet at the three stages, $\phi = \phi_{\text{iv}} + \phi_{\text{㈡}} + \phi_{\text{㈢}}$.

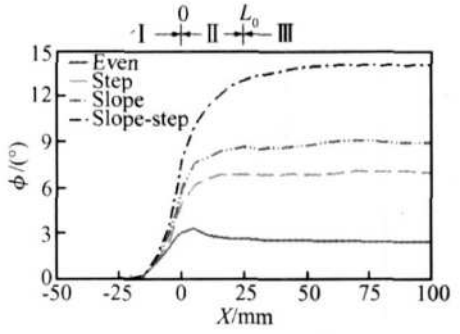

Fig. 10 Evolution of vectoring angle ϕ, which is divided into three stages

4 Conclusions and future work

The interactions between a primary jet and four types of actuator with different exits are numerically simulated. And the evolution of vectoring control of a primary jet with synthetic jets was investigated.

The evolution of jet vectoring using synthetic jets is divided into three stages, and the final vectoring angle of the primary jet is a total result of the primary jet controlled by synthetic jet at the three stages, $\phi = \phi_{\text{iv}} + \phi_{\text{㈡}} + \phi_{\text{㈢}}$. In the conduit of the primary jet ($X \leqslant 0$), the low-pressure region, which results from the interaction between the synthetic jet and the primary jet, contributes to the vectoring force and leads to a turning of the primary jet at the conduit exit, and the primary jet turns ϕ_{iv}. And then, in the near field ($0 \leqslant X \leqslant L_0$), the primary jet fluid is entrained and absorbed by the synthetic jet during the blowing and the suction stroke, and the primary jet turns $\phi_{\text{㈡}}$, $\phi_{\text{㈡}}$ is complicated and may be a positive, zero or negative value, and the jet vectoring is nearly finished in this field. Finally, in the far field ($X \geqslant L_0$), the shear layer of primary jet is inspirited by the vortices of synthetic jet, and the primary jet turns $\phi_{\text{㈢}}$, $\phi_{\text{㈢}}$ is a small value and negligible.

The use of synthetic jet actuation for thrust vectoring shows great promise; however, it is still in a primary development stage. While success has been achieved numerically, the applications have been small scale and simplified. Further research is necessary before synthetic jet actuation can be applied to air-breathing engines to provide large-scale fluidic thrust vectoring. In the future, a quantitative model of vectoring control of a primary jet with synthetic jets is also necessary, and the evolution of jet vectoring control provides a base for modeling a quantitative model.

References

[1] Kowalh J. Advances in thrust vectoring and the application of flow-control technology [J]. *Canadian Aeronautics and Space Journal*, 2002, 48(2).

[2] Glezer A., Amitay M. Synthetic jets [J]. *Ann. Rev. Fluid Mech.*, 2002, 34.

[3] 罗振兵, 夏智勋. 合成射流技术及其在流动控制中应用的进展 [J]. 力学进展, 2005, 35(2).

[4] Smith B L, Glezer A. Vectoring and small-scale motions affected in free shear flows using synthetic jet actuators [R]. *AIAA* 97-0213.

[5] Smith B L, Glezer A. Jet vectoring using synthetic jets [J]. *J. Fluid Mech.*, 2002, 458.

[6] Guo D H, Cary A. Numerical simulation of vectoring control of a primary jet with synthetic jet [J]. *AIAA J.*, 2003, 41(12).

[7] Luo Z B, Zhu B P, Xia Z X, et al. Jet vectoring using synthetic jet actuators [J]. *Journal of Propulsion Technology*, 2004, 25(5). (罗振兵, 朱伯鹏, 夏智勋, 等. 合成射流激励器对射流矢量的影响 [J]. 推进技术, 2004, 25(5).)

[8] 高 峰, 汪 亮, 张志峰. 单微射流作动器控制主流参

数分析 [J]. 空军工程大学学报, 2005, 6(1).

[9] Luo Z B, Xia Z X. An optimal mode of jet vectoring using synthetic jet actuators [C]. *The 8th International Symposium on Fluid Control, Measurement and Visualization*, 2005, *Chengdu, China*.

[10] Li N, Zhang K Y, Xu J L. Experimental investigation of primary flow vectoring using parallel synthetic jets [J]. *Journal of Propulsion Technology*, 2005, 26(3). (李念, 张堃元, 徐惊雷, 等. 自耦合射流对平行主射流的矢量偏转实验研究 [J]. 推进技术, 2005, 26(3).)

[11] Luo Z B, Xia Z X. The mechanism of jet vectoring using synthetic jet actuators [J]. *Modern Physics Letters B*, 2005, 19(28, 29).

[12] Wang H, Menon S. Fuel-air mixing enhancement by synthetic micro-jets [J]. *AIAA J.*, 2001, 39(12).

[13] Mittal R, Rampunggoon P. On the virtual aero-shaping effect of synthetic jets [J]. *Physics of Fluids*, 2002, 14(4).

[14] Luo Z B, Xia Z X. A novel valve-less synthetic jet based micro-pump [J]. *Sensors Actuators A*, 2005, 122(1).

[15] Lee C, Hong G. A piezoelectrically actuated micro synthetic jet for active flow control [J]. *Sensors and Actuators A.*, 2003, 108 (1~3).

[16] Luo Z B, Xia Z X, HU J X, et al. Numerical simulation of synthetic jet flow field and parameter analysis of actuator [J]. *Journal of Propulsion Technology*, 2004, 25(3). (罗振兵, 夏智勋, 胡建新, 等. 合成射流流场数值模拟及激励器参数分析 [J]. 推进技术, 2004, 25(3).)

[17] 罗振兵. 合成射流流动机理及其应用研究 [D]. 长沙: 国防科技大学, 2002.

(编辑: 刘萝威)

(上接第 178页)

[4] Stephens S E, Bates L B. Effect of geometric parameters on the performance of second throat annular steam ejectors [R]. *ADA* 238645, 1991.

[5] Kim S, Kwon S. Experimental determination of geometric parameters for an annular injection type supersonic ejector [J]. *Journal of Fluids Engineering-Transactions ASME*, 2006, 128: 1164~1171.

[6] Emanuel G. Optimum performance for a single-stage gaseous ejector [J]. *AIAA Journal* 1976, 14(9): 1292~1296.

[7] 张堃元, 沈炳炎. 主流倾斜的引射器试验研究 [J]. 航空动力学报, 2000, 15(4): 439~441.

[8] 王广振, 吴寿生. 王之珊, 等. 混合管面积和位置对排气引射器性能的影响 [J]. 推进技术, 2000, 21(4). (WANG Guang-zhen, WU Shou-sheng, WANG Zhi-shan, et al. Effect of mixing tube area and position on performances for lobed ejector [J]. *Journal of Propulsion Technology*, 2000, 21(4).)

[9] Tillman T G, Paterson R W, Presz W M. Supersonic nozzle mixer ejector [J]. *Journal of Propulsion and Power*, 1992, 8(2): 513~519.

[10] Hu H, Kobayashi T, Saga T, et al. Research on the rectangular lobed exhaust ejector/mixer systems [J]. *Transactions of The Japan Society for Aeronautical and Space Sciences*, 1999, 41(134): 187~194.

[11] 凌其扬, 廖达雄. 风洞引射器试验研究 [J]. 气动实验与测量控制, 1994, 8(2): 10~18.

[12] Hale J W. Influence of pertinent parameters on ejector-diffuser performance with and without ejected mass [R]. *ADA* 602770, 1964.

[13] 廖达雄, 任泽斌, 余永生, 等. 等压混合引射器设计与实验研究 [J]. 强激光与粒子束, 2006, 18(5): 728~732.

[14] 缪亚芹, 王锁芳, 吴恒刚. 多喷管引射器试验研究与数值模拟 [J]. 南京师范大学学报 (工程技术版), 2006, 6(2): 67~71.

[15] Jones W L, Price H S, Lorenzo C F. Experimental study of zero-flow ejectors using gaseous nitrogen [R]. *NASA-TN-D-203*, 1960.

(编辑: 刘萝威)